VTT Technical Research Centre of Finland

Drainage of high-consistency fiber-laden aqueous foams

Koponen, Antti I.; Timofeev, Oleg; Jäsberg, Ari; Kiiskinen, Harri

Published in:
Cellulose

DOI:
10.1007/s10570-020-03416-y

Published: 11/09/2020

Document Version
Publisher's final version

License
CC BY

Cellulose (2020) 27:9637–9652
https://doi.org/10.1007/s10570-020-03416-y

ORIGINAL RESEARCH

Drainage of high-consistency fiber-laden aqueous foams

Antti I. Koponen · Oleg Timofeev · Ari Jäsberg · Harri Kiiskinen

Received: 14 April 2020 / Accepted: 22 August 2020 / Published online: 11 September 2020

Abstract Lightweight lignocellulosic fibrous materials (LLFMs) offer a sustainable and biodegradable alternative in many applications. Enthusiastic interest in these materials has recently grown together with the newly risen interest in foam forming. Foam bubbles restrain fiber flocculation, and foam formed structures have high uniformity. Moreover, the bubbles support the fibrous structure during manufacturing enabling the formation of highly porous structures. Mechanical pressure cannot be applied in the manufacture of LLFMs as the materials would lose their porous structure. Water is therefore typically removed by a combination of drainage and thermal drying. Thermal drying of porous materials has been studied intensively. However, there are only a few studies on the drainage of fiber-laden foams. Thus, in this work, we conducted a systematic analysis of this topic. Our findings show that after drainage a stationary vertical moisture profile similar to that of pure foams is developed. Raising the initial fiber consistency was found to increase the final fiber consistency of the foam until the drainage ceased. Increasing mold height was found to increase the final consistency considerably. Without vacuum and heating, the shrinkage of samples during drainage was only slightly higher than the volume of the drained water. Drainage rate and final consistency increased clearly with increasing vacuum, but simultaneously sample shrinkage increased considerably. The best compromise was obtained with a vacuum of 0.5 kPa, which increased the final consistency by 60% without extra shrinkage. Using warm foam and heating the foam during drainage increased the final consistency considerably, but this also led to significant shrinkage of the sample.

Keywords Fiber-laden foam · Foam forming · Drying · Drainage · Lightweight cellulose materials · Lightweight fibrous structures

A. I. Koponen (✉) · O. Timofeev · A. Jäsberg · H. Kiiskinen
VTT Technical Research Centre of Finland, P.O. Box 1603, 40101 Jyväskylä, Finland
e-mail: Antti.Koponen@vtt.fi

Introduction

Lightweight lignocellulosic fibrous materials (LLFMs) offer a sustainable and biodegradable alternative in many applications such as thermal insulation (Pöhler et al. 2017), sound insulation (Nechita and Năstac 2018; Debeleac et al. 2019), interior decoration (Härkäsalmi et al. 2017; Siljander et al. 2019), polymer-impregnated composites, and packaging (Satyanarayana et al. 2009; Huber et al. 2012). As lignocellulosic fibers have strong aggregation tendency, LLFMs are difficult to produce with conventional water forming. However, due to the recent

resurgence of foam forming, interest in these materials is now growing rapidly.

In foam forming, fibers are mixed with water and surfactants to create a fiber-laden foam with a typical air content of 50–70% (Punton 1975a, b; Smith and Punton 1975; Smith et al. 1974; Poranen et al. 2013; Koponen et al. 2016b; Lehmonen et al. 2020). The bubbles restrain flocculation in the foam, and the formed structures obtain much better uniformity than achieved with water. Moreover, the bubbles support the fibrous structure during manufacturing, enabling the production of highly porous structures with densities lower than 10 kg/m^3 (Korehei et al. 2016; Burke et al. 2019). Finally, much higher consistencies can be used with foam when compared to water, which gives improved energy and water efficiency.

When making LLFMs with aqueous foams, water is usually removed from the fibrous structures in two steps. The first step is dewatering (drainage), in which water flows in the fiber-laden foam downwards due to gravity and is removed at the bottom of the sample. After drainage, the capillary pressure and gravity are in balance and the foam has a stationary moisture profile. The second step is thermal drying, in which the remaining water is removed from the structure by evaporation. Mechanical pressure cannot be used in either step as the samples would lose their porous structure. However, low vacuum can be used to speed up the process and make it more efficient. Porous cellulosic structures can also be produced with other methods, such as freeze-drying (Cervin et al. 2012; Korehei et al. 2016; Josset et al. 2017), supercritical carbon dioxide drying (Sehaqui et al. 2011) and air-drying from volatile organic solvents (Wege et al. 2008). However, these methods are hardly viable for commercial low-cost large-scale production of LLFMs.

Thermal drying of porous structures is a technological problem that has been studied intensively (Kowalski, 2007; Xu et al. 2019). Considerable knowledge has been gained on thermal drying of foam-like materials in the food industry (Hertzendorf et al. 1970; Kudra and Ratti 2006; Sangamithra et al. 2015) and thermal drying of fibrous structures in the paper industry (Stenström 2020) and nonwoven industry (Lyons and Vollers 1971). Although LLFMs are novel materials, there are already a few studies dedicated to their thermal drying. Thermal drying of LLFMs has been studied at room temperature by Korehei et al. (2016), Nechita and Năstac (2018), and Burke et al. (2019), and at higher temperatures by Alimadadi and Uesaka (2016), Pöhler et al. (2017), and Härkäsalmi et al. (2017). Moreover, Timofeev et al. (2016) have studied thermal drying of LLMFs with infrared heating in combination with vacuum and impingement drying (hot air jet).

The drainage process of pure foams has been studied extensively (Verbist et al. 1996; Koehler et al. 2000, 2006; Stevenson 2006; Kruglyakov et al. 2008, 2010; Papara et al. 2009; Arjmandi-Tash et al. 2015; Koursari et al. 2019). However, there are few studies on the drainage of fiber-laden foams (Haffner et al. 2017). Analysis of the drainage of fiber-laden foams is therefore relevant from both a practical and academic point of view. There is also a lack of studies of the effect of vacuum on the drainage of fiber-laden foams (Korehei et al. 2016). Such studies, however, have significant practical relevance for optimization of the dewatering phase to save both time and energy during thermal drying.

In this work, we systematically analyze the drainage of fiber-laden foams. We study the effect of initial fiber consistency, fiber type and mold height on the final consistency and shrinkage of fiber-laden foams. In addition, we analyze the effect of vacuum and heating on drainage and shrinkage.

Materials and methods

Three pulps were used as the raw material for the fibrous samples: virgin pine fiber (average length-weighted length 2.1 mm), virgin birch fiber (0.9 mm), and chemi-thermomechanical pulp (CTMP, CSF 600, 2.0 mm). The fiber lengths have been measured with L&W FiberMaster Plus. In the experiments, the fiber consistency was varied from 2 to 8%. (Fiber consistency is obtained by dividing the mass of dry fibers with the mass of dry fibers and water combined). Sodium dodecyl sulfate (SDS, purity at least 90%) surfactant was used as the foaming agent.

The foams were made at room temperature ($T \sim$ 18–22 °C) from tap water with an SDS dosage of 0.6 g/l. The critical micelle concentration for SDS is 2.38 g/l in ion-exchanged water at 25 °C. Due to the presence of ions, the critical micelle concentration is here considerably lower, ca. 1.5 g/l (Lehmonen et al. 2020). The surface tension was $\sigma \approx 35$ mN/m. The

effect of SDS on viscosity is rather small. At an SDS dosage of 4 g/l, the viscosity of the SDS solution is less than 4% higher than pure water, which is at 20 °C 1.0 mPas (Kushner et al. 1952).

The foams were produced by mixing the fiber suspension and surfactant with air in a tank (tank diameter 125 mm, height 430 mm). A circular disc with a diameter of 83 mm and two opposing 25 degree bends was used as the mixing blade. Mixing was improved by moving the impeller up and down during mixing. Mixing speed was 3500 rpm and mixing time was 15 min. The air fraction of the produced foam was 65–70% which is the typical range used in real-life applications of foam forming (Punton 1975a; Lehmonen et al. 2020). To maximize the porosity of the final fibrous network air content should be as high as possible. On the other hand, the foam should still be liquid-like to be easily processable. Monodisperse foam experiences a jamming transition at the air content of 64% (Saint-Jaimes and Durian 1999). For polydisperse foam jamming transition takes place with a slightly higher air content.

The Sauter mean diameter of foam bubbles is defined as

$$r_{32} = \frac{\sum_{i=1}^{n} f_i r_i^3}{\sum_{i=1}^{n} f_i r_i^2}, \quad (1)$$

where f_i and r_i are, respectively, the number and radius of bubbles in a particular size fraction i. Sauter mean radius reflects the size of identical spherical bubbles, a system of which has the same total surface area and total volume as a system of multisized bubbles (Kowalczuk and Drzymala 2016). The total surface energy of the monosized bubbles is then equal to the total surface energy of polysized bubbles. As surface energy is a fundamental quantity for foams, Sauter mean radius is widely used for describing the mean size of bubbles. Figure 1 shows the Sauter mean radius of bubbles as a function of consistency. Bubble size was measured using the method presented by Lappalainen and Lehmonen (2012). Here a cuvette with 1.6 mm spacing between two glass plates is used for foam collection by dipping the cuvette into foam. The cuvette is lit from behind using a fibre optic backlight panel and imaged with a CCD-camera. The bubble size is determined from the images by using the circular Hough transform. We can see in Fig. 1 that bubble radius reaches equilibrium with increasing consistency, being ca. 55–60 µm when the consistency exceeds 4%. Notice that the bubble radius is 15–35 times smaller than the typical fibre size.

After mixing, the foam was poured into cylindrical molds with an inner diameter of 165 mm. The height of the single-ring molds varied from 10 to 100 mm (for examples see Fig. 2a). Using molds with different heights made it possible to analyze the drainage process with different sample thicknesses (see Fig. 2b). Drainage time was in most cases ca. 25 min. A metal screen (stainless steel mesh) in the bottom of the molds retained the fibers while allowing the water to run out of the molds with low resistance. The water runoff was collected and its mass was recorded at 0.5 Hz frequency using a digital laboratory balance. In some cases, the time evolution of the thickness of the samples was also recorded with laser line profiling using a frequency of 2.5 Hz. Notice that this setup cannot be used for analyzing the drainage of pure foams, as pure foams pass through the metal screen.

Figure 3 shows a comparison of drainage and drainage rate of a fiber-laden foam (air content 70%) and a water-fiber suspension as a function of time for CTMP pulp in a 40 mm mold. In both cases the initial consistency is 3% and the amount of water is the same. Foam and water are seen to behave very differently. The drainage rate of water is initially very high (five times that of foam) but it decreases rapidly. As a result, the samples made with foam have a much higher final consistency even though the initial consistencies are equal. Foam forming has great potential for the manufacture of porous fiber-based products; not only due to the ability to make low-density uniform structures, but also due to improving the dryness of the produced (wet) fibrous samples.

A seven-ring mold with a height of 140 mm was used to analyze the vertical consistency profile of the sample after drainage (see Fig. 4). The target height in making the rings was 20 mm. In practice the variation of ring heights was ± 0.5 mm. The inner diameter of rings was 100 mm. The mold was filled to the brim with fiber foam, and drainage was completed in 35 min. After drainage, each ring was removed separately, and the fiber-foam was skimmed from the mold with a thin metal plate onto aluminum plates. The wet fiber-foam samples were weighed, dried in an

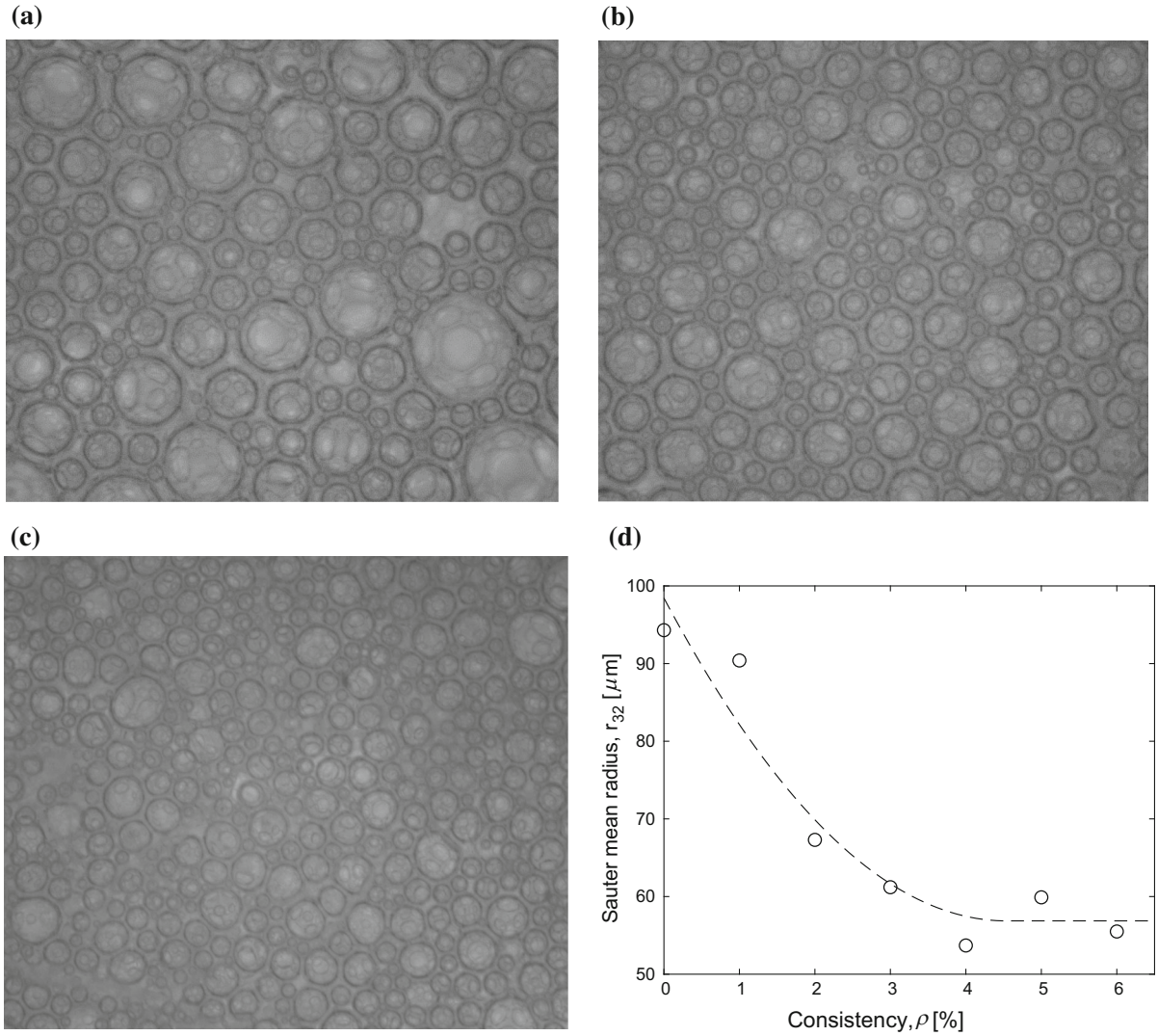

Fig. 1 Microscopic images (1.7 mm × 2.0 mm) of aqueous foam samples taken from the mixing tank: **a** Pure foam. **b** Fiber consistency 2.0%. **c** Fiber consistency 6.0%. **d** Sauter mean radius of bubbles as a function of consistency. Dashed line is a visual guide. Notice that the bubble radius is 15–35 times smaller than the typical fibre length

oven at 105 °C, and then reweighed. Three measurements were performed with pine fiber with initial consistencies of 4.3%, 3.2% and 3.6% (the last with 0.5 kPa vacuum). During drainage the sample shrank in the seven-ring mold by approximately 30 mm; by the end the top ring was empty and only 50–75% of the following ring was filled with fiber-foam (see Fig. 5). The fiber content of the other rings was approximately equal. Free drainage thus did not seem to create a significant height-dependent fiber density profile in the sample. When a low vacuum was used the number of fibers was slightly higher in the bottom ring compared to the other rings. Note that Burke et al. (2019) observed at the sample top and bottom a ca. 3 mm layer of higher fiber concentration. We did not examine this in our study, but our samples are assumed to have a similar structure. It is also noteworthy that, unlike our study and that of Burke et al. (2019), Haffner et al. (2017) studied the liquid drainage using a closed mold, which resulted in a sharp downward gradient of fiber concentration. The reason for this behavior is unclear. Finally notice that the fibre content in ring 2 was slightly reduced. This is probably due to the height of this ring being slightly

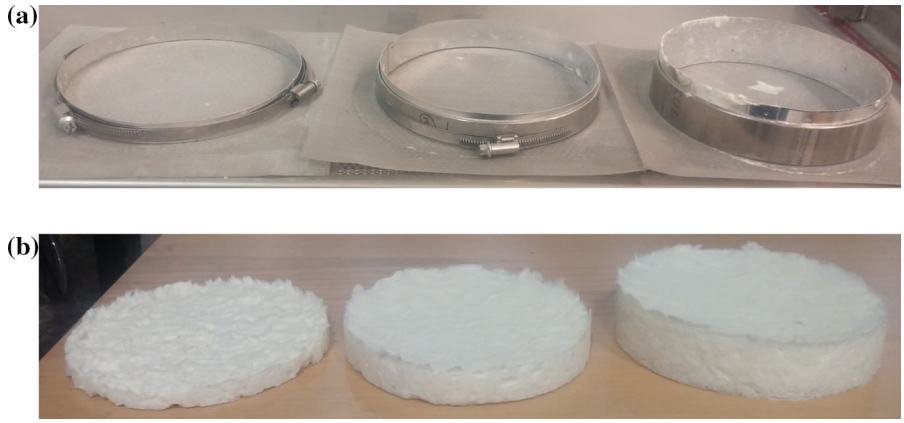

Fig. 2 **a** Examples of used molds. Height from left to right: 15 mm, 25 mm and 40 mm. Inner diameter 165 mm. **b** Examples of final drained and dried samples made with the above molds

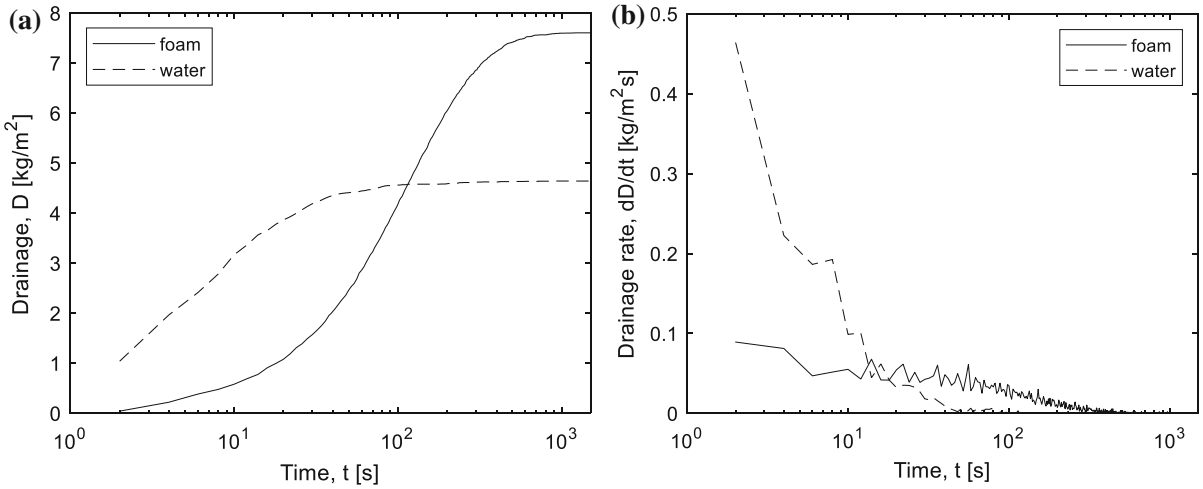

Fig. 3 Comparison of **a** drainage (mass of drained water per unit area) and **b** drainage rate of a fiber-laden foam and a fiber-water suspension as a function of time. Consistency of the CTMP fiber is 3% and the mold height is 40 mm. Final consistency is 7.0% for foam and 4.5% for water

smaller compared to the other rings. However, we can't rule out other reasons such as an imperfect filling of the mold.

Drainage can be accelerated by increasing the temperature of the fiber-laden foam or by using a vacuum. Increased temperature reduces water viscosity. As a result, the water flow resistance of the fiber-foam structure is lowered, enabling water to flow more easily through it. Further improvement of drainage can be achieved by creating an upward temperature gradient across the foam. The resulting thermocapillary Marangoni effect creates a surface tension gradient that accelerates the downward flow of water (Miralles et al. 2014).

The effect of vacuum, foam temperature and heating on drainage was studied with the setup shown in Fig. 6. The measurement device comprised a mold fitted with a metal screen at the bottom, a measuring column, and a rubber seal. The measuring column was connected to a vacuum pump, and vacuum under the sample mold was measured. The amount of drained liquid was measured with a ruler. Foam temperature was measured using a K-type thermocouple located at the bottom of the sample mold. In some cases, the fiber mass was first heated to 50–55 °C and then foamed.

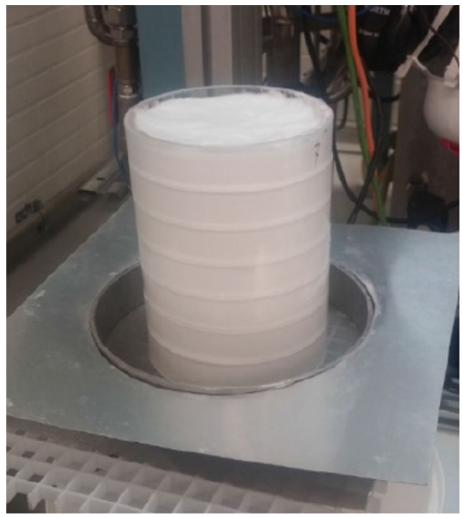

Fig. 4 Seven-ring mold used for vertical consistency analysis. Mold height 140 mm

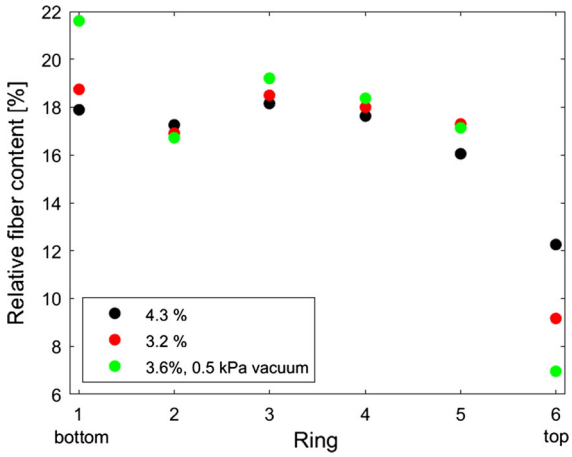

Fig. 5 Relative fiber content per ring (sum of all rings is 100%) in the seven-ring mold after drainage with and without low vacuum. 1 = bottom ring, 6 = ring below the top ring. The sample compressed during drainage; thus ring 7 was empty and ring 6 only partly filled. Some experimental variations in relative consistencies were present, but free drainage does not seem to create a significant height-dependent fiber density profile in the sample. With low vacuum, relative consistency is slightly higher in the bottom ring compared to the other rings

The warm fiber foam was then poured into the sample mold. Cooling of the heated foam could be slowed during drainage using an infra heater installed above the sample mold (this also created an upward temperature gradient in the foam). In these tests, pine fiber was used at 2.0% initial consistency. The mold height was 80 mm.

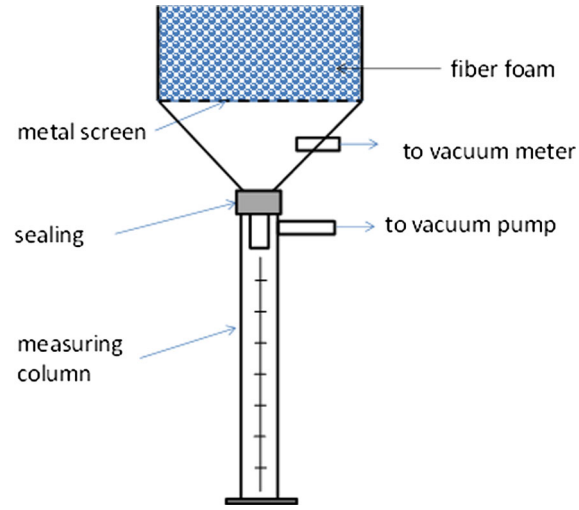

Fig. 6 Schematic of the mold with vacuum at the bottom

Results

Effect of initial consistency on drainage

The effect of initial consistency on drainage was studied with CTMP furnish in a 40 mm mold. Table 1 shows for these trial points the initial height of the sample i.e. mold height, H_m, the initial consistency, ρ_i, final consistency, ρ_f, the amount of water removed, w, the total shrinkage of the sample height, Δh, the shrinkage of the sample height due to the leakage of air, Δh_{air}, and the initial air content, φ. Initial air content was calculated using the formula:

$$\varphi = 1 - \left[(m_{\text{wet}} + m_{\text{d}} - m_{\text{dry}})/\rho_w + m_{\text{dry}}/\rho_p\right]/Ah_i, \tag{2}$$

where A is the cross sectional area of the mold, h_i is the initial height of the sample, m_{wet} is the mass of the wet sample after drainage, m_{d} is the mass of drained water, m_{dry} is the mass of the sample after drying, ρ_w = 1000 kg/m^3 is the density of water, and ρ_p = 1500 kg/m^3 is the density of pulp fiber. Shrinkage of the sample height due do air leakage was calculated from $\Delta h_{\text{air}} = \Delta h - m_{\text{d}}/A\rho_w$.

We can see from Table 1 that final consistency increases gradually with increasing initial consistency. Figure 7 shows the consistency change $\Delta\rho = \rho_f - \rho_i$ as a function of initial consistency ρ_i. The dashed line shows a linear fit $\Delta\rho = -0.71\rho_i + 5.9$ with the data points. When $\Delta\rho = 0$, this formula gives $\rho_i = 8.3\%$. It

Table 1 Trial points of the drainage experiments with variable initial consistency

TP	Furnish	H_m(mm)	ρ_i(%)	ρ_f(%)	w(%)	Δh(%)	Δh_{air}(%)	φ(%)
1	CTMP	40	2.9	7.0	61	21.4	0.8	65
2	CTMP	40	3.0	6.5	55	23.1	4.6	66
3	CTMP	40	3.2	6.8	55	–	–	–
4	CTMP	40	3.7	7.0	50	19.6	4.7	69
5	CTMP	40	5.0	7.6	36	–	–	–
6	CTMP	40	5.1	7.3	32	11.5	2.2	70
7	CTMP	40	5.7	7.4	24	10.3	3.6	71
8	CTMP	40	6.8	7.7	13	4.8	1.0	70
9	CTMP	40	7.0	8.0	13	8.6	4.8	70
10	CTMP	40	7.5	8.1	8	3.9	1.5	69

Left to right: trial point, furnish, mold height (H_m), initial consistency (ρ_i), final consistency (ρ_f), amount of water removed (w), total sample height shrinkage (Δh), sample height shrinkage due to air leakage (Δh_{air}), and initial air content (φ). The height change has been measured with laser profiling

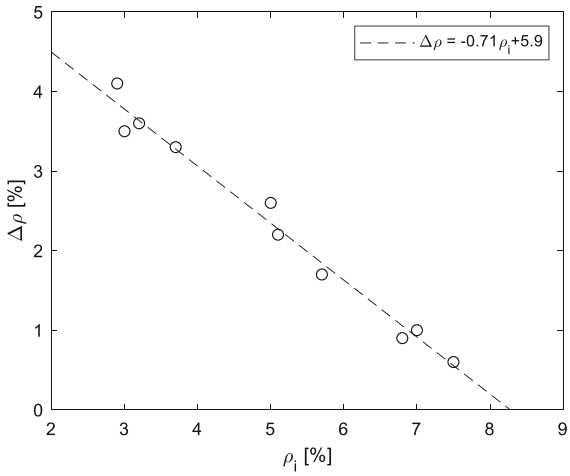

Fig. 7 Consistency change $\Delta\rho = \rho_f - \rho_i$ as a function of initial consistency ρ_i

is likely that with higher initial consistencies drainage would be negligibnle with this mold height.

Figure 8 shows the drainage and drainage rate as a function of time for various consistencies. Note that, due to experimental noise, the drainage rate curves have been obtained by filtering the original data with Matlab's smooth function using a Savitzky–Golay filter with a 20-point window. We can see from Fig. 8b that initially there is a short transient phase of ca. 20 s during which the drainage rate increases. After that, the drainage rate decreases monotonically.

After the initial transient phase, ending at time t_0, drainage follows very accurately with all consistencies the formula ($R^2 > 0.98$, see dashed lines in Fig. 8a):

$$D = M\left(1 - e^{(t_o - t)/T}\right),\ t > t_0. \tag{3}$$

Parameter T, which gives the time scale of the drainage process, is approximately equal, $T \sim 130$ s, in all cases. The dynamics of the drainage process is thus independent of the initial consistency. Notice that Eq. (3) gives as the drainage rate.

$$\frac{dD}{dt} = \frac{M}{T} e^{(t_o - t)/T},\ t > t_0. \tag{4}$$

Drainage rate thus decreases exponentially as a function of time. We can see from Fig. 8b that Eq. (4) works well after the initial transient phase. Notice that (Cox et al. 2000) showed that in the later phase, drainage rate of pure foams decreases exponentially with time. Our results suggests that for fiber-laden foams exponential decay is a good approximation for the whole drainage process.

Compression during drainage

As Table 1 shows, the fiber foam samples compressed during drainage. With highest initial consistencies sample compression is less than 10%, while with lowest consistencies compression is up to 23%. Figure 9a shows the time development of sample thickness during drainage. Figure 9b compares the

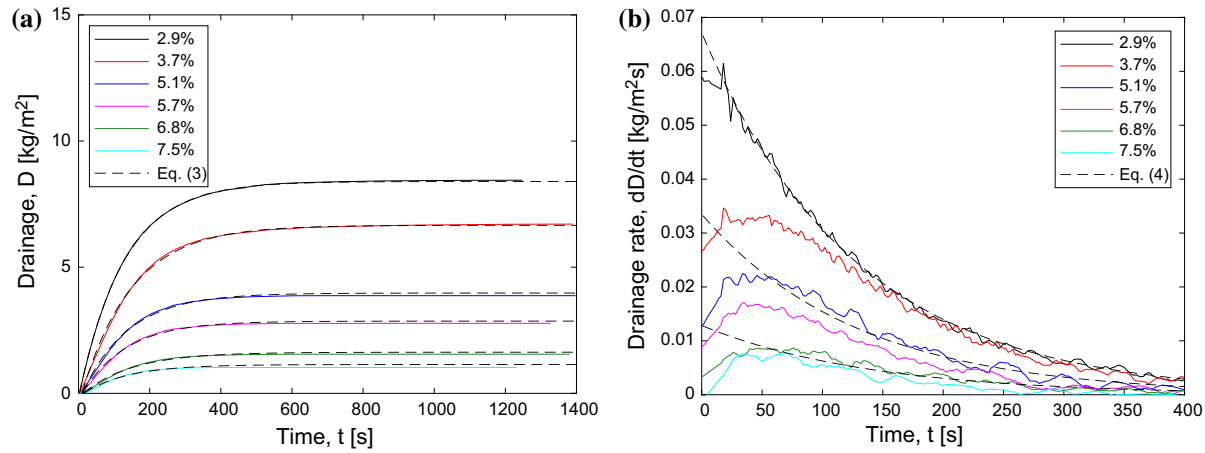

Fig. 8 **a** Drainage, **b** drainage rate as a function of time for CTMP pulp with various initial consistencies. The dashed lines in **a** and **b** are the fits of Eqs. (3) and (4) to the measured drainage and drainage rate curves, respectively. Mold height 40 mm

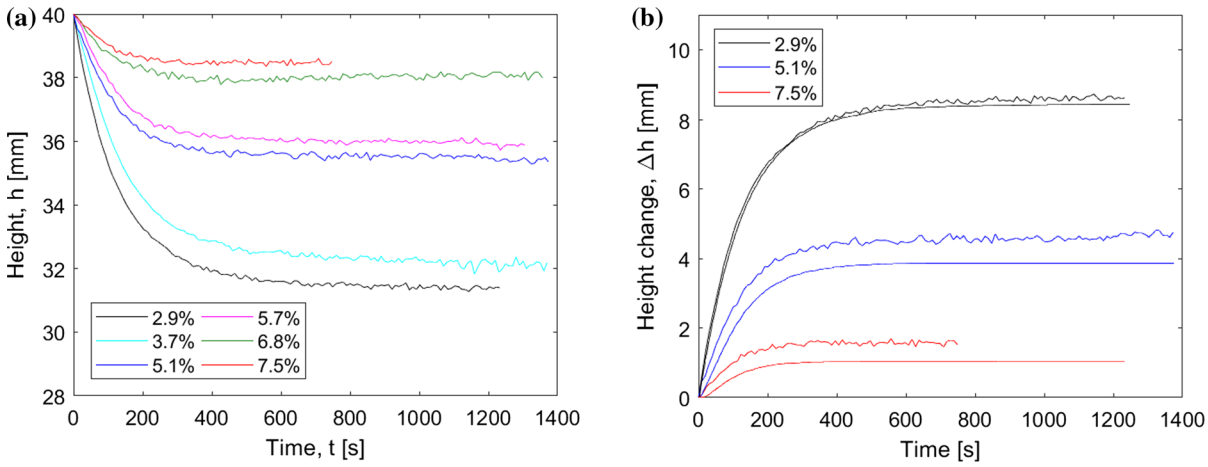

Fig. 9 **a** Sample height as a function of time for various initial consistencies of CTMP pulp. Mold height 40 mm. Initial sample height varied from 40–43 mm. The profiles are normalized to start at h = 40.0 mm to facilitate reading the graph. **b** Measured change in sample height (fluctuating lines) and height change calculated from drained water (smooth lines)

change in sample height with that calculated from the volume of drained water. We can see from Fig. 9b that the sample compression is due to both water draining and leakage of air. The decrease in sample height due to air leakage varies between 1–5%, and no systematic dependence on initial consistency is seen. Most bubbles thus seem to remain intact during drainage, supporting the fibrous structure and preventing its collapse.

For the trial points shown in Table 1, compression is linearly dependent on initial consistency (R^2 = 0.95):

$$\Delta h_{\%} = -4.0\rho_i + 33.7\%. \quad (5)$$

(Above ρ_i and $\Delta h_{\%}$ are expressed in percentages.) Notice that Eq. (5) is in line with the shrinkage observed for pine fibers when the 7-ring mold was used. As we did not always perform height measurement during drainage, we used Eq. (5) below in some cases to estimate the final sample height after drainage.

The height measurement data can be used for analyzing the geometrical properties of the structure of the final sample. Figure 10 shows the solids density, ρ_s, and porosity of the final drained samples before drying when the remaining water is omitted from the analysis. (We have, i.e., assumed that all residual

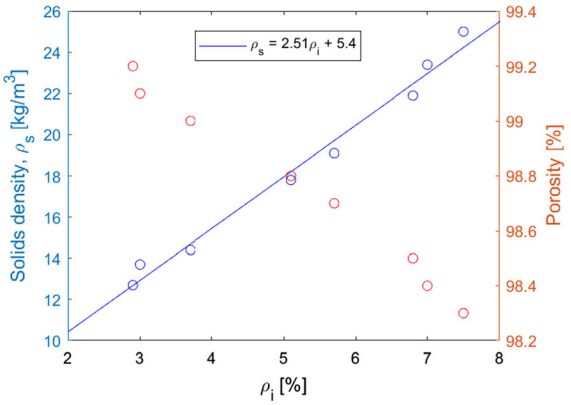

Fig. 10 Solids density and porosity of the final CTMP samples as a function of initial consistency, with the assumption that all residual water has been removed without changing the sample structure. Mold height 40 mm

water has been removed without changing the 3D structure of the sample.) Porosity has been calculated from the solids density by assuming that the density of fibers is 1500 kg/m^3. We see from Fig. 10 that the samples are very porous before drying and solids density is a linear function of initial density.

$$\rho_s = 2.51\rho_i + 5.4. \quad (6)$$

Above, ρ_i is expressed in percentages and ρ_s in kg/m^3. Note that by extrapolating Eq. (6) to very dilute initial consistencies ($\rho_i \rightarrow 0$), one gets ρ_s = 5.4 kg/m^3. This is close to the density of pine fiber networks, ρ_s = 4 kg/m^3, obtained with foam forming and freeze drying with 0.5% initial consistency and a 20 mm mold (Korehei et al. 2016). Burke et al. (2019) used pine fiber with a 50 mm mold and dried the samples for 40 h at room temperature. With an air content of 67% and initial fiber density of 1.0%, the solids density of the dry samples was 8.8 kg/m^3, which is well in line with Eq. (6).

Table 2 shows the furnish, mold height, initial consistency, final consistency, and the amount of removed water, for the drainage experiments made with mold heights of 10–100 mm. Consistency was approximately constant, varying between 3.1 and 3.8% and averaging at 3.4%. A linear regression analysis of the data shown in Table 1 gives for final consistency (R^2 = 0.98)

$$\rho_f = 5.6 + 0.044H_m + \beta, \quad (7)$$

Table 2 Drainage experiments conducted with mold heights of 10–100 mm. Initial consistency was kept constant, but in practice varied between 3.1–3.8%.

TP	Furnish	H_m (mm)	ρ_i (%)	ρ_f (%)	w (%)
11	Pine	10	3.3	4.5	28
12	Pine	20	3.4	6.2	46
13	Pine	30	3.5	6.9	51
14	Pine	40	3.4	7.8	58
15	Pine	60	3.1	8.3	65
16	Pine	80	3.2	9.3	68
17	Pine	100	3.2	10.0	70
18	Birch	10	3.6	4.4	19
19	Birch	20	3.6	5.2	31
20	Birch	30	3.7	5.9	38
21	Birch	40	3.5	6.1	44
22	Birch	60	3.5	7.0	51
23	Birch	80	3.6	7.8	56
24	Birch	100	3.7	8.3	57
25	CTMP	10	3.4	5.1	34
26	CTMP	20	3.8	4.8	23
27	CTMP	30	2.8	4.6	41
28	CTMP	40	3.3	6.1	47
29	CTMP	60	3.1	7.3	58
30	CTMP	80	3.3	8.0	61
31	CTMP	100	3.3	8.8	64

Left to right: trial point, furnish, mold height, initial consistency, final consistency, and amount of removed water. Note that trial points 28–30 are averages over two measurements

where β is is zero for pine, − 1.4 for birch, and − 1.2 for CTMP. Consistency is expressed in Eq. (7) in percentages and mold height in millimeters. Note that trial points 11 and 27 were outliers and were omitted from the regression analysis. For other trial points, Eq. (7) works very well, and the relative difference between the modelled final consistency and the measured final consistency is always less than 0.1. On average, the relative difference is only 0.03.

Effect of mold height on final consistency

We see from Eq. (7) that final consistency increases with increasing mold height. As we see below, this can be explained by a consistency profile that is developed during drainage. Pine has a more than one percentage

point higher final consistency than birch and CTMP. This is probably due to pine fibers having larger diameter and smaller specific surface area than birch and CTMP fibers. Thus, the average pore size of pine samples is probably bigger (this decreases the capillary pressure) and the available wetting surface is smaller (there is less room for water to be absorbed) than for birch and CTMP.

Figure 11 shows the consistency in each ring of the seven-ring mold. We see that there is a vertical consistency profile in the samples. Consistency increases monotonically from bottom to top and the profiles for the two non-vacuum measurements are very similar. When a low vacuum is used, consistency increases more in the vicinity of sample bottom. At the top the effect of the vacuum is minimal.

Figure 12 shows the final consistency as a function of sample height. The data for 10–100 mm molds is for pine fiber. The final sample heights for the 10–100 mm molds were obtained from Eq. (5). The 7-ring data presented in Fig. 12 is cumulative; the consistency at a given height is an average over the rings below that point. We can see that the different data sets agree very well with each other. Final consistency increases systematically with increasing sample height.

When pure foam is in contact with the drained water the dependence of volumetric water content

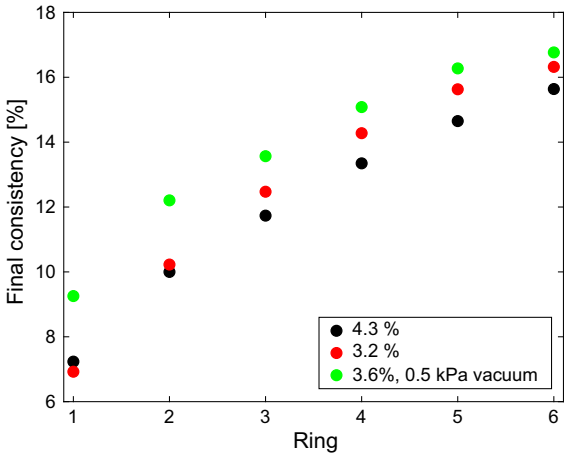

Fig. 11 Final consistency in each ring of the seven-ring mold after drainage. 1 = bottom ring, 6 = ring below the top ring. Consistency increases monotonically from bottom to top. With low vacuum consistency increases more at the bottom of the sample. Pine fiber was used. Initial consistencies are given in the legend

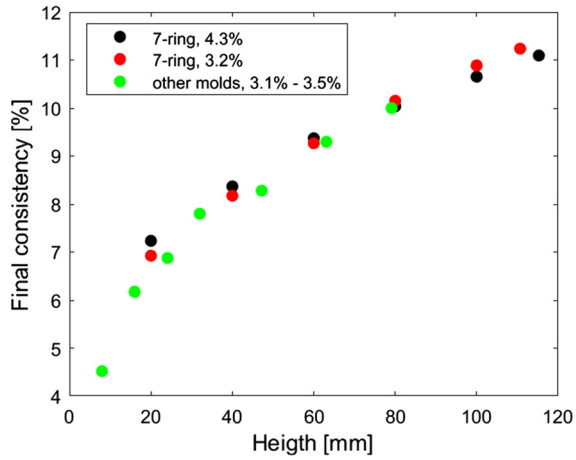

Fig. 12 Final consistency as a function of sample height. 10–100 mm molds and seven-ring mold data are shown. Shrinkage differed slightly between the two seven-ring samples, which explains the slightly different position of the highest data point. Pine fiber was used. Initial consistencies are given in the legend

(liquid fraction) on height, z, at the end of the drainage process is obtained from the formula (Haffner et al. 2017):

$$\phi_{\mathrm{eq}}(z) = \left[\frac{1}{\sqrt{\phi_c}} + \sqrt{3}\frac{r_{32}}{\lambda_c^2} z\right]^{-2}, \tag{8}$$

where $\phi_c = 0.36$ is the water content below which the foam has a yield stress, r_{32} is the bubble radius, and $\lambda_c = \sqrt{\sigma/\rho g}$ is the capillary length (here σ is the surface tension, and ρ is the density of water). When deriving Eq. (8) it is assumed that the bubble size does not change during drainage (no coarsening or coalescence). While this assumption is an approximation, it is quite reasonable here as fibers slow down coalescence (Mira et al. 2014; Li et al. 2016).

Figure 13 shows with r_{32} = 60 µm (see Fig. 1) the liquid fraction as a function of vertical position, z, in the sample for a pure foam together with the measured liquid fractions for fiber foams using the seven-ring mold. The theoretical and experimental profiles are rather similar. In our setup, the draining fiber foam is not in contact with the drained water. The metal screen, however, may hold some water in its voids creating an effective water boundary at the bottom of the mold. This may be one reason for the similarity of the curves shown in Fig. 13.

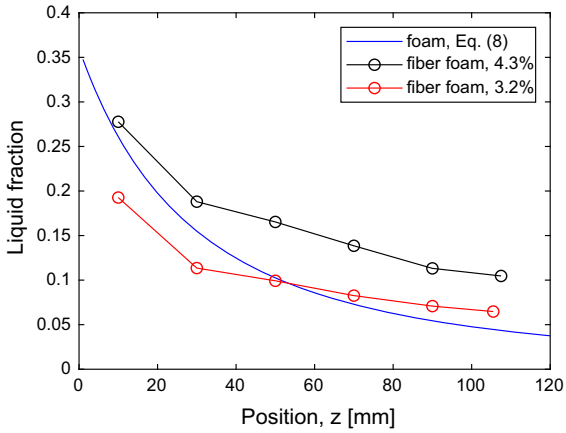

Fig. 13 Local liquid fraction as a function of vertical position after drainage for pure foam (see Eq. (8)) together with the measured liquid fractions for fiber-laden foams. The measurement was performed with the seven-ring mold using pine fiber

For pure foam that is in contact with water the final liquid fraction after drainage is (Haffner et al. 2017):

$$\overline{\phi}_{\mathrm{eq}} = \frac{\lambda_c^2\sqrt{\phi_c}}{\sqrt{3}Hr_{32}}\left[1 - \frac{1}{1+\sqrt{3}H\frac{r_{32}}{\lambda_c^2}\sqrt{\phi_c}}\right], \tag{9}$$

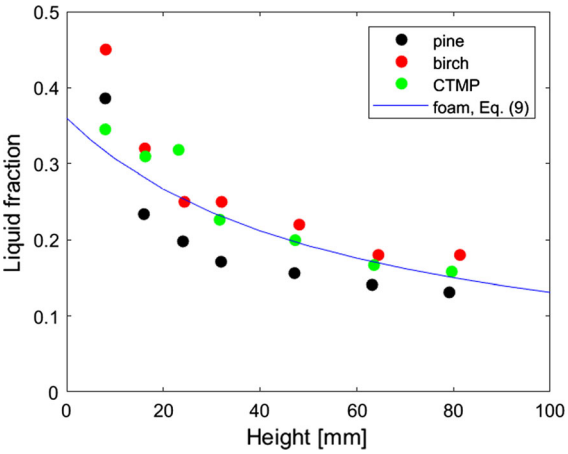

Fig. 14 Theoretical liquid fraction (see Eq. 9) of pure foam and the measured liquid fractions for fiber foams made with the 10–100 mm molds from pine (initial consistency ca. 3.3%), birch (initial consistency ca. 3.6%) and CTMP (initial consistency ca. 3.3%) as a function of final sample height (calculated from Eq. 5)

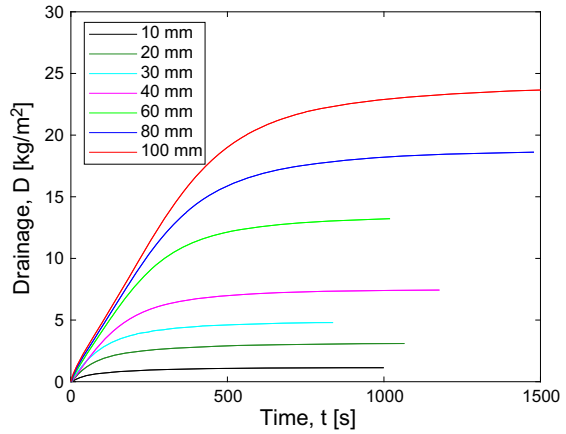

Fig. 15 Drainage as a function of time for various mold heights for pine. Initial consistency was on average 3.3%

where H is the sample height. Figure 14 shows the theoretical liquid fraction together with the measured results for pine, birch and CTMP with r_{32} = 60 µm. The agreement between the theoretical prediction for pure foams and the experimental data is quite good.

Drainage dynamics with different mold heights

Figure 15 shows drainage as a function of time for pine fiber (trial points 11–17) with different mold heights. Birch and CTMP behaved qualitatively very similarly. We saw above that the time evolution of drainage could be given by Eq. (3) for a mold height of 40 mm with good accuracy. Although drainage dynamics is more complicated for higher molds (see

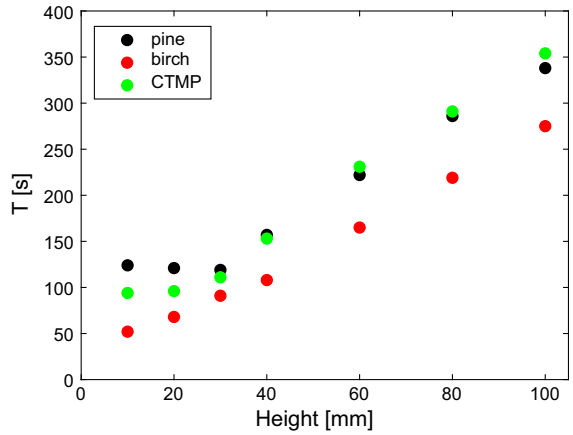

Fig. 16 Values of parameter T of Eq. (3) fitted to the drainage data for different furnishes and mold heights

below), Eq. (3) can still be used for describing general drainage behavior. Figure 16 shows values of parameter T for the fit of Eq. (3) to the drainage data for different furnishes and mold heights. We can see from Fig. 16 that the drainage process takes significantly longer (higher values of T) with increasing mold height and that the process is clearly faster for birch than for pine and CTMP. We currently have no explanation for this behavior. When the mold height is 40 mm or higher, T increases linearly with approximately the same slope with all three furnishes.

Figure 17 shows the drainage rate of pine as a function of time. We see from Fig. 17 that initially there is a short transient phase of the order of 10 s where the drainage rate increases from zero to its maximum value. The drainage rate then starts to decrease exponentially with the 10–40 mm mold heights. With mold heights of 60–100 mm, the behavior is more complex. After reaching its peak value, the drainage rate drops rapidly during the next 20 s. Then, for a while, the drainage rate is approximately constant; e.g. for the 100 mm mold this phase takes about 250 s. Finally, the drainage rate starts to decrease exponentially. Koponen et al. (2018) studied the initial drainage rate for 1.5% pine fiber foams in a closed container; at 65 and 70% air content, drainage rates were 0.072 kg/m^{2}s and 0.057 kg/m^{2}s, respectively. These values are closely in line with our observed peak values for the 60–100 mm molds (see inset in Fig. 17a).

We compared the drainage curves shown in Fig. 17 with those obtained by solving the classical drainage equation for pure foams presented, for example, by Verbist et al. (1996) and Haffner et al. (2017). The qualitative behavior of drainage given by the model was similar to the measured behavior: with high mold heights the drainage rate peaked at the beginning of the process, and the drainage rate was then approximately constant before decreasing exponentially. With smaller molds the drainage rate started to decrease exponentially immediately. The time scale of drainage given by the model was, however, almost an order of magnitude longer than in the experiments. The time scales could be matched by multiplying the effective fluid viscosity by a free scaling parameter as was done by Haffner et al. (2017). The authors cannot, however, rigorously justify this method by the known properties of the system, thus it would be a pure numerical trick to circumvent the difference between the model and the experiments. So, while the final stationary state of aqueous foam and fiber-laden foam appear to be similar (see Figs. 13 and 14) the dynamics of drainage is quantitatively different. New models are therefore evidently needed for quantitative description of the drainage of fiber-laden foams. For this purpose, we have offered all of the drainage measurements as open data (https://zenodo.org/record/3585554). We encourage readers to use these data as a basis for developing new models for the drainage of fiber-laden foams.

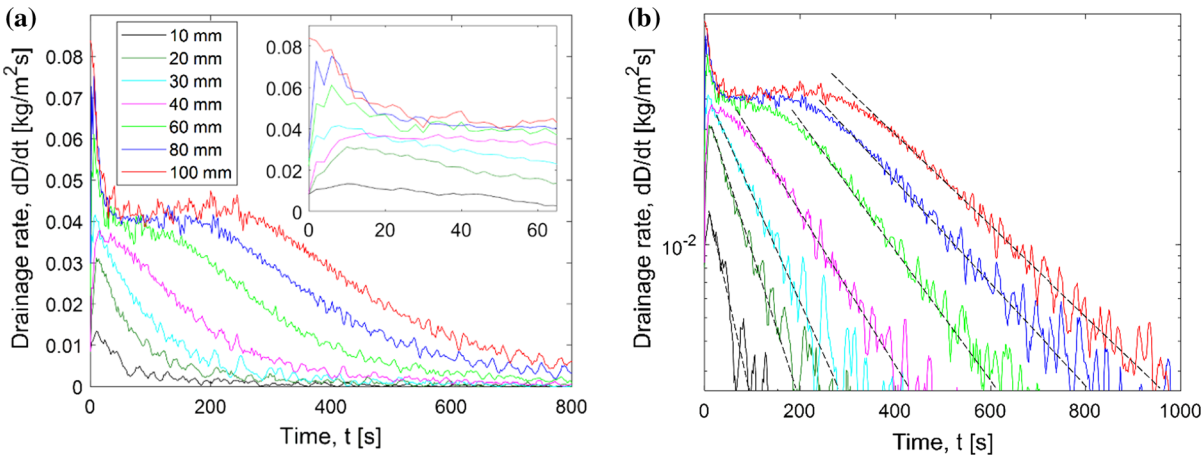

Fig. 17 Drainage rate for pine as a function of time for different mold heights in **a** linear scale, **b** log-lin scale. The inset in Figure **a** shows the drainage rate during the first 65 s. With mold heights of 60, 80 and 100 mm, the drainage process consists of four phases: peak drainage rate, constant drainage rate, transient phase, and exponentially decreasing drainage rate (see dashed straight lines in **b**

Table 3 Drainage experiments conducted with different vacuum levels (0–5 kPa). In trials 46–48 the foam was initially heated to 50–55 °C. For trial 48, the foam was also heated with infrared radiation during the drainage process

TP	Furnish	H_m (mm)	p (kPa)	ρ_i (%)	ρ_f (%)	w (%)	Δh (%)	Δh_{air} (%)
32	pine	80	0	2.1	8.2	76	25	3.2
33	pine	80	0.5	2.1	12.8	86	28	3.1
34	pine	80	1	2.1	14.5	86	28	2.3
35	pine	80	2	2.1	15.5	86	34	7.9
36	pine	80	3	2.1	17.6	88	38	9.8
37	pine	80	4	2.2	19.9	89	44	17
38	pine	80	5	2.2	22.0	90	50	25
39	birch	80	0	2.1	7.6	72	25	4.1
40	birch	80	0.5	2.3	12.9	83	28	3.8
41	birch	80	1	2.2	15.3	86	31	7.0
42	birch	80	2	2.2	16.3	86	35	9.6
43	birch	80	3	2.2	17.1	87	38	12
44	birch	80	4	2.1	16.3	87	40	16
45	birch	80	5	2.3	17.9	87	44	19
46	pine	80	0 (hot)	1.9	8.1	78	33	11
47	pine	80	0.5 (hot)	2.2	13.7	86	36	12
48	pine	80	0.5 (inf.)	2.3	19.1	90	35	10

Initial consistency was ca. 2.2%. Left to right: trial point, furnish, mold height, vacuum and heating (hot = initial heating of foam, inf. = initial heating of foam + infrared heating), initial consistency, final consistency, amount of removed water, total shrinkage of the sample, and shrinkage of the sample due to air leakage. The height change has been measured with a ruler

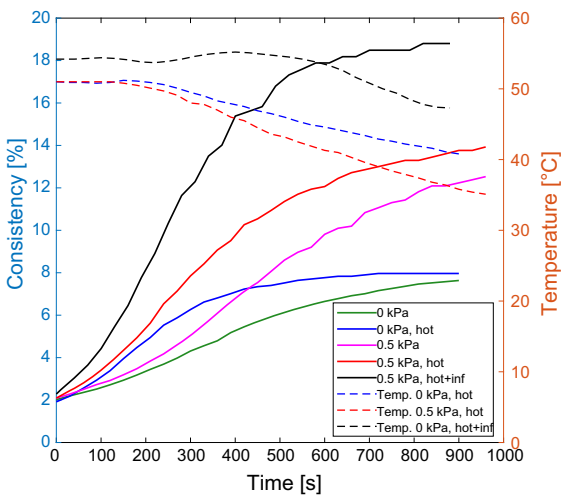

Fig. 18 Effect of vacuum level and heating on drainage of pine fiber foam. The foam temperature during drainage is also shown. Initial consistency is ca. 2.0% and the mold height is 80 mm

Effect of low vacuum and fiber foam temperature on drainage

Table 3 shows the trials points where the vacuum level was varied between 0–5 kPa. Most trials were performed at room temperature, but for trials 46, 47 and 48 the foam was initially heated to 50–55 °C. At trial point 48 the foam was also heated during the drainage process with an infrared lamp.

Figure 18 shows the time evolution of consistency for pine for different vacuum and heating conditions. Due to decreasing water viscosity, heating increases the drainage rate considerably both with and without 0.5 kPa vacuum.

Figure 19a shows the effect of vacuum and heating on the final consistency. We see in Fig. 19a that consistency is clearly improved when vacuum is used, but the benefit decreases with increasing vacuum level. With birch, final consistency starts to saturate already with a vacuum of 3 kPa. Heating the foam is

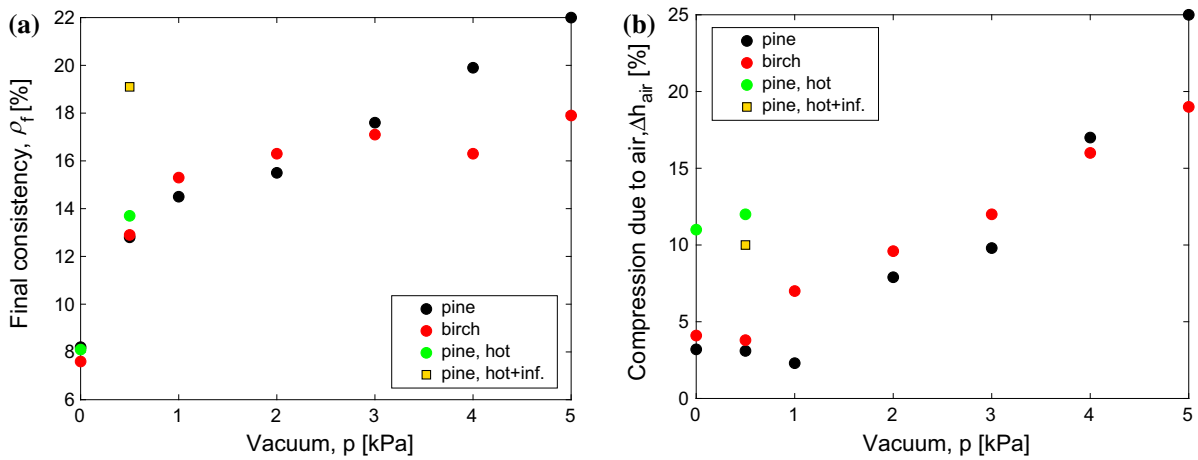

Fig. 19 Effect of vacuum and heating on **a** final consistency and **b** compression of the sample due to leakage of air. Initial consistency ca. 2.2% and mold height 80 mm

seen to have only a minor effect on the final consistency unless the foam is also heated during the drainage process. In that case, the final consistency is significantly increased to the same level as with the highest vacuums. Notably, the consistencies obtained with the highest vacuum are similar to those seen in paper machines after the forming board (Koponen et al. 2016a, b).

As discussed above, the samples compress during drainage by at least as much as the volume of drained water. In addition to this, some extra compression takes place due to leakage of air out of the sample. Figure 19b shows the effect of vacuum and heating on the compression of the sample due to leakage of air. We can see in Fig. 19b that Δh_{air} is similar with and without a 0.5 kPa vacuum. With higher vacuum levels compression increases, reaching about 20% with the highest vacuum of 5 kPa. We also see in Fig. 19b that heating the foam increases compression significantly.

Conclusions

Foam forming is a promising method for making lightweight lignocellulosic fibrous materials. Unlike water, the bubbles in foam support the fibrous structure during manufacturing, enabling the formation of highly porous structures. As mechanical pressure cannot be used, it is important to remove as much water as possible from the fibrous structures by drainage before thermal drying. Timofeev et al. (2016) have shown that shrinkage of the structures during thermal drying can be eliminated by choosing the right drying conditions. Minimizing the shrinkage of the sample during drainage is thus critical for the successful manufacture of LLFM structures.

In addition to analyzing free drainage, we studied the effect of vacuum and heating of foam on drainage. We found that by the end of drainage a stationary vertical moisture profile is developed that is similar to that of pure foams. Rising initial consistency increased the final consistency of the foam until drainage ceased. Increasing the mold height increased the final consistency considerably. Without application of vacuum and heating, sample shrinkage during drainage was only slightly higher than the volume of the drained water. Drainage rate and final consistency increased clearly with increasing vacuum, but at the same time sample shrinkage increased considerably. The best compromise was obtained with a vacuum of 0.5 kPa, which increased the final consistency by 60% without extra shrinkage. Using warm foam and heating the foam during drainage increased the final consistency considerably, but this also led to significant shrinkage of the sample. Due to the wide parameter space of this work it was not possible to perform several parallel measurements with identical process parameters. The observed trends, however, are always very consistent and there are few outliers. The accuracy and repeatability of the results should thus to be rather good.

Future studies should investigate possibilities for strengthening the fibrous structures to allow higher

vacuums and higher foam temperatures. One option is to add small amounts of cellulose nanofibrils to the structure (Cervin et al. 2013). The drainage process can also possibly be further optimized by using increasing vacuum as a function of time. This could minimize sample shrinkage during drainage.

Acknowledgments This work was conducted as part of the Future Fibre Products 2020 (FFP2020) project, which is funded by the European Regional Development Fund (Grant Nos. A73089, A73092), VTT Technical Research Centre of Finland Ltd, and 32 industrial partners.

Funding Open access funding provided by Technical Research Centre of Finland (VTT).

Data availability Open data: https://zenodo.org/record/3585554

Complaince with ethical standards

Conflict of interest The authors declare that they have no conflict of interest.

References

Alimadadi M, Uesaka T (2016) 3D-oriented fiber networks made by foam forming. Cellulose 23(1):661–671. https://doi.org/10.1007/s10570-015-0811-z

Arjmandi-Tash O, Kovalchuk N, Trybala A, Starov V (2015) Foam drainage placed on a porous substrate. Soft Matter 11(18):3643–3652. https://doi.org/10.1039/c5sm00377f

Burke S, Möbius M, Hjelt T, Hutzler S (2019) Properties of lightweight fibrous structures made by a novel foam forming technique. Cellulose 26(4):2529–2539. https://doi.org/10.1007/s10570-018-2205-5

Cervin NT, Aulin C, Larsson P, Wågberg L (2012) Ultra porous nanocellulose aerogels as separation medium for mixtures of oil/water liquids. Cellulose 19:401–410. https://doi.org/10.1007/s10570-011-9629-5

Cervin N, Andersson L, Ng J, Olin P, Bergström L, Wågberg L (2013) Lightweight and strong cellulose materials made from aqueous foams stabilized by nanofibrillated cellulose. Biomacromolecules 14(2):503–511. https://doi.org/10.1021/bm301755u

Cox S, Weaire D, Hutzler S, Murphy J, Phelan R, Verbist G (2000) Applications and generalizations of the foam Drainage equation, proceedings: mathematical. Phy Eng Sci 456:2441–2464

Debeleac C, Nechita P, Nastac S (2019) Computational investigations on soundproof applications of foam-formed cellulose materials. Polymers 11(7):1–20. https://doi.org/10.3390/polym11071223

Haffner B, Dunne F, Burke S, Hutzler S (2017) Ageing of fibre-laden aqueous foams. Cellulose 24(1):231–239. https://doi.org/10.1007/s10570-016-1100-1

Härkäsalmi T, Lehmonen J, Itälä J, Peralta C, Siljander S, Ketoja J (2017) Design-driven integrated development of technical and perceptual qualities in foam-formed cellulose fibre materials. Cellulose 24(11):5053–5068. https://doi.org/10.1007/s10570-017-1484-6

Hertzendorf M, Moshy R, Seltzer E (1970) Foam drying in the food industry. C R C Crit Rev Food Technol 1:25–70. https://doi.org/10.1080/10408397009527099

Huber T, Müssig J, Curnow O, Pang S, Bickerton S, Staiger M (2012) A critical review of all-cellulose composites. J Mater Sci 47(3):1171–1186. https://doi.org/10.1007/s10853-011-5774-3

Josset S, Hansen L, Orsolini P, Griffa M, Kuzior O, Weisse B, Zimmermann T, Geiger T (2017) Microfibrillated cellulose foams obtained by a straightforward freeze–thawing–drying procedure. Cellulose 24(9):3825–3842. https://doi.org/10.1007/s10570-017-1377-8

Koehler S, Hilgenfeldt S, Stone H (2000) A generalized view of foam drainage: experiment and theory. Langmuir 16(15):6327–6341. https://doi.org/10.1021/la9913147

Koponen A, Torvinen K, Jäsberg A, Kiiskinen H (2016b) Foam forming of long fibers. Nord Pulp Pap Res J 31(2):239–247. https://doi.org/10.3183/npprj-2016-31-02-p239-247

Koponen A, Haavisto S, Liukkonen J, Salmela J (2016a) The flow resistance of fiber sheet during initial dewatering. Drying Technol 34(12):1521–1533. https://doi.org/10.1080/07373937.2015.1132427

Koponen A, Jäsberg A, Lappalainen T, Kiiskinen H (2018) The effect of in-line generation of foam on the foam quality and the sheet formation in foam forming. Nord Pulp Pap Res J 33(3):482–495. https://doi.org/10.1515/npprj-2018-3051

Korehei R, Jahangiri P, Nikbakht A, Martinez M, Olson J (2016) Effects of drying strategies and microfibrillated cellulose fiber content on the properties of foam-formed paper. J Wood Chem Technol 36(4):235–249. https://doi.org/10.1080/02773813.2015.1116012

Koursari N, Arjmandi-Tash O, Johnson P, Trybala A, Starov V (2019) Foam drainage placed on a thin porous layer. Soft Matter 15(26):5331–5344. https://doi.org/10.1039/c8sm02559b

Kowalczuk P, Drzymala J (2016) Physical meaning of the Sauter mean diameter of spherical particulate matter. Part Sci Technol 34(6):645–647. https://doi.org/10.1080/02726351.2015.1099582

Kowalski S (ed) (2007) Drying of porous materials. Springer, Newyork

Kruglyakov P, Karakashev S, Nguyen A, Vilkova N (2008) Foam drainage. Curr Opin Coll Interface Sci 13(3):163–170. https://doi.org/10.1016/j.cocis.2007.11.003

Kruglyakov P, Elaneva S, Vilkova N, Karakashev S (2010) Investigation of foam drainage using foam pressure drop technique. Coll Surf A 354(1–3):291–297. https://doi.org/10.1016/j.colsurfa.2009.06.014

Kudra T, Ratti C (2006) Foam-mat drying: energy and cost analyses. Can Biosyst Eng 48:27–32

Kushner L, Duncan B, Hoffman J (1952) A viscometric study of the micelles of sodium dodecyl sulfate in dilute solutions. J Res Nat Bur Stand 49(2):85–90

Lappalainen T, Lehmonen J (2012) Determinations of bubble size distribution of foam-fibre mixture using circular hough transform. Nord Pulp Pap Res J 27(5):930–939. https://doi.org/10.3183/NPPRJ-2012-27-05-p930-939

Lehmonen J, Retulainen E, Paltakari J, Kinnunen-Raudaskoski K, Koponen A (2020) Dewatering of foam-laid and water-laid structures and the formed web properties. Cellulose 27(3):1127–1146. https://doi.org/10.1007/s10570-019-02842-x

Li S, Xiang W, Järvinen M, Lappalainen T, Salminen K, Rojas O (2016) Interfacial stabilization of fiber-laden foams with carboxymethylated lignin toward strong nonwoven networks. ACS Appl Mater Interfaces 8(30):19827–19835. https://doi.org/10.1021/acsami.6b06418

Lyons D, Vollers C (1971) The drying of fibrous materials. Text Res J 41(8):661–668

Miralles V, Selva B, Cantat I, Jullien M (2014) Foam drainage control using thermocapillary stress in a two-dimensional microchamber. Phys Rev Lett 112(23):1–5. https://doi.org/10.1103/PhysRevLett.112.238302

Mira I, Andersson M, Boge L, Blute I, Carlsson G, Salminen K, Lappalainen T, Kinnunen K (2014) Foam forming revisited Part I Foaming behaviour of fibre-surfactant systems. Nord Pulp Pap Res J 29(04):679–689

Nechita P, Năstac S (2018) Foam-formed cellulose composite materials with potential applications in sound insulation. J Compos Mater 52(6):747–754. https://doi.org/10.1177/0021998317714639

Papara M, Zabulis X, Karapantsios T (2009) Container effects on the free drainage of wet foams. Chem Eng Sci 64(7):1404–1415. https://doi.org/10.1016/j.ces.2008.11.021

Pöhler T, Jetsu P, Fougerón A, Barraud V (2017) Use of papermaking pulps in foam-formed thermal insulation materials. Nord Pulp Pap Res J 32(3):367–374. https://doi.org/10.3183/npprj-2017-32-03-p367-374

Poranen J, Kiiskinen H, Salmela J, Asikainen J, Keränen J, Paakkonen E (2013) Break-through in papermaking resource efficiency with foam forming. In: Proceedings of TAPPI PaperCon, Atlanta, GA, USA, 807–814.

Punton V (1975a) Fibre distribution in foam and foam-laid paper. Int Paper Physics Conf 135–139

Punton V (1975b) The use of an aqueous foam as a fibre-suspending medium in quality papermaking. In: Proceedings of a Symposium Organized by the Society of the Chemical Industry. Colloid and Surface Chemistry Group 179–194. Brunel University

Saint-Jaimes A, Durian D (1999) Vanishing elasticity for wet foams: equivalence with emulsions and role of polydispersity. J Rheol 43:1411–1422. https://doi.org/10.1122/1.551052

Saint-Jalmes A (2006) Physical chemistry in foam drainage and coarsening. Soft Matter 2(10):836–849. https://doi.org/10.1039/b606780h

Sangamithra A, Venkatachalam S, John S, Kuppuswamy K (2015) Foam mat drying of food materials: a review. J Food Process Preserv 39(6):3165–3174. https://doi.org/10.1111/jfpp.12421

Satyanarayana K, Arizaga G, Wypych F (2009) Biodegradable composites based on lignocellulosic fibers—an overview. Prog Polym Sci 34(9):982–1021. https://doi.org/10.1016/j.progpolymsci.2008.12.002

Sehaqui H, Zhou Q, Ikkala O, Berglund L (2011) Strong and tough cellulose nanopaper with high specific surface area and porosity. Biomacromolecules 12(10):3638–3644. https://doi.org/10.1021/bm2008907

Siljander S, Keinänen P, Ivanova A, Lehmonen J, Tuukkanen S, Kanerva M, Björkqvist T (2019) Conductive cellulose based foam formed 3D shapes—from innovation to designed prototype. Materials 12(3):1–12. https://doi.org/10.3390/ma12030430

Smith M, Punton V (1975) Foam can improve formation. Pulp Paper Canada 76(1):55–58

Smith M, Punton V, Rixson A (1974) The structure and properties of paper formed by a foaming process. Tappi J 57(1):107–111

Stenström S (2020) Drying of paper: a review 2000–2018. Drying Technol 38(7):825–845. https://doi.org/10.1080/07373937.2019.1596949

Stevenson P (2006) Dimensional analysis of foam drainage. Chem Eng Sci 61(14):4503–4510. https://doi.org/10.1016/j.ces.2006.02.026

Timofeev O, Jetsu P, Kiiskinen H, Keränen J (2016) Drying of foam-formed mats from virgin pine fibers. Drying Technol 34(10):1210–1218. https://doi.org/10.1080/07373937.2015.1103254

Verbist G, Weaire D, Kraynik A (1996) The foam drainage equation. J Phys Cond Matt 8(21):3715–3731. https://doi.org/10.1088/0953-8984/8/21/002

Wege H, Kim S, Paunov V, Zhong Q, Velev O (2008) Long-term stabilization of foams and emulsions with in-situ formed microparticles from hydrophobic cellulose. Langmuir 24(17):9245–9253. https://doi.org/10.1021/la801634j

Xu P, Sasmito A, Mujumdar A (2019) Heat and Mass Transfer in Drying of Porous Media. CRC Press, Boca Raton